Development of a Noise Reduction Approach for Vibration–based Damage Detection Involving High-order Derivatives

Hao XU** Li CHENG** and Zhongqing SU**
**The Department of Mechanical Engineering, The Hong Kong Polytechnic University, Kowloon, Hong Kong SAR
* E-mail: mmsu@polyu.edu.hk

Abstract
To enhance the sensitivity of vibration-based identification techniques to damage of relatively small dimension, it is a common practice to explore higher-order derivatives of a captured vibration signal. However the measurement noise and uncertainties, inevitably contained in a vibration signal, can be fairly exacerbated during the differentiation process towards higher-order derivatives, masking damage-associated signal features and posing difficulty in signal interpretation. The objective of the present work is to examine variations of random measurement noise in such a differentiation process. A quantitative description of the noise influence, subject to various mathematic factors during the differentiation including differential intervals and initial noise level, was derived. A signal processing method based on low-pass wavenumber filtering was developed, to facilitate the de-noising treatment. As proof-of-concept validation, the proposed approach was employed to reduce measurement noise in vibration signals during detection of damage in a structural beam component. Thanks to the diversity of de-noising options, enhanced identification precision and accuracy over traditional de-noising endeavors was obtained.

Key words: Vibration-based damage detection, Noise reduction, High-order derivative, Signal processing

1. Introduction

Various damage detection methods based on examining structural mode shape and its derivatives have been intensively studied in recent decades with demonstrated effectiveness and efficiency [1, 2]. However, along with the increase in the derivative order, the interference due to measurement noise and uncertainties, which cannot be avoided in practical applications, tends to be more and more serious, sometime leading to a failure of the identification.

A damage detection technique recently developed by the authors [3], based on locally canvassing the dynamic equilibrium relationships across monitored structure components, was verified both numerically and experimentally. The most appealing advantage of the approach is its independence of a series of prerequisites that cannot be circumvented in traditional vibration-based detection techniques, such as the needs of prior knowledge on the state of intact counterpart structures and boundary conditions. However, the fourth-order derivatives of the vibration deflection involved in the expression of the proposed damage index make this approach extremely sensitive to measurement noise and uncertainties. This concern is ubiquitous in most vibration-based damage detection approaches in which

higher-order derivatives of the captured responses are involved. Thus, to develop effective de-noising treatments claims its vital significance towards practical applications.

In this paper, two de-noising techniques, adjustment of measurement configuration (AMC) and low-pass wavenumber filtering (LWF), were developed, respectively, to eliminate the noise influence on the higher-order derivatives of vibration responses. Moreover, thanks to the diversity of de-noising techniques, a plenty of data can be formed through a very limited number of tests, and a further improvement of detection results can be realized through data fusion. The feasibility of the developed de-noising treatments was validated experimentally on a simple cantilever structural beam.

2. Construction of Damage Index

In a recently developed damage detection approach based on locally examining the relationship of dynamic equilibrium of the structure under inspection [3], a damage index, for a beam component for example, was constructed according to the equation of motion, defined as:

$$DI = EI\frac{d^4w(x)}{dx^4} - \rho S\omega^2 \cdot w(x) \tag{1}$$

where $w(x)$ is the transverse vibration displacement of the beam component at x; E, ρ, I and S are the complex Young's modulus (including material damping), density, area moment of inertia and cross-section area of the beam; ω is the angular frequency of the excitation. The higher-order derivatives in Eq. (1) can be calculated using closely spaced measurements (for example from point *i-2* to *i+2*) across the entire beam in terms of the following finite difference scheme:

$$DI_i = \frac{EI}{D_m^4}\left(w_{i+2} - 4w_{i+1} + 6w_i - 4w_{i-1} + w_{i-2}\right) - \rho S\omega^2 w_i \tag{2}$$

where DI_i is the damage index at measurement point i; D_m is the distance between two adjacent measurement points.

Using a cantilever beam with a small damaged zone for illustration, the finite element (FE) model for the beam is presented in Fig. 1. The beam is 600*mm* long, 20*mm* wide and 10*mm* thick. The complex Young's Modulus is $70\times(1+10^{-4}i)$ *GPa* (the structural damping was included in the imaginary part), and the density is $2700\ kg/m^3$. The beam was evenly meshed by 3840 solid elements. The through-width damaged zone was centralized at x=460*mm* from the clamped end, and its length is 10*mm* along the beam span (about 1.7% of the total beam length). Compared to the rest of the beam, there is a 2*mm* reduction in the thickness within the damaged zone. The flexural velocity at every single measurement point was captured from the intact surface of the beam, opposite to which lay the damage. A single point excitation was located at x=100*mm* to generate vibration signals. In order to eliminate the influence of external excitation on identification, an inspection region, from x=200*mm* to x=600*mm* ($L_{inspection}$=400*mm*) was selected by excluding the vicinity of the point of excitation, as shown in Fig. 1. Damage indices within this inspection region were constructed.

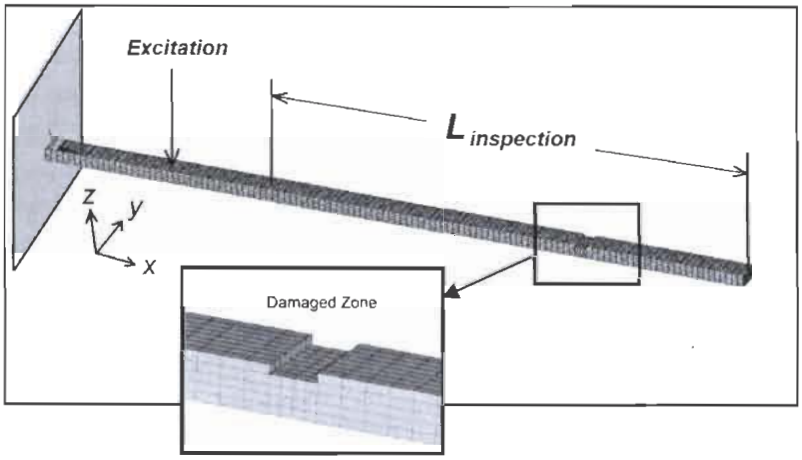

Fig. 1 FE model for a cantilever beam containing a damaged zone

Under the excitation frequency of 900*Hz*, selected on a random basis, the distribution of vibration deflection in the absence of any perturbation from measurement noise is shown in Fig. 2(a), and the constructed damage indices DI^{exact} using Eq. (2) was presented by the solid line in Fig. 2(b), from which the local drastic changes can be observed clearly, showing the position and length (along the beam span) of the damaged zone. In contrast, noise influence was introduced in the exact deflection in accordance with:

$$w^{noisy} = w^{exact}\Delta w e^{j\Delta\varphi} \tag{3}$$

where w^{exact} and w^{noisy} are the vibration deflections of the beam without and with added noise, respectively; Δw a Gaussian random real number related to magnitude of w^{exact}; $\Delta\varphi$ another Gaussian random real number related to phase. The accordingly constructed damage index is denoted by DI^{noisy}, compared with DI^{exact} in Fig. 2(b) using the dashed line when Δw is 1% of the magnitude of w^{exact}, and $\Delta\varphi$ is 1°. It can be seen, under the interference of added noise, the calculated DI^{noisy} presents poor recognizability because the information pertaining to damage is fairly masked by noise.

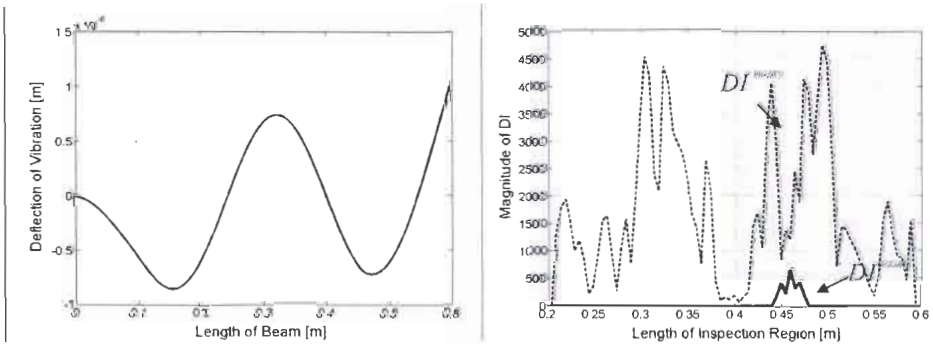

(a) (b)

Fig. 2 (a) Vibration deflection and (b) accordingly constructed damage indices with and without the interference of noise (the number of measurement points was 121 across the whole beam span)

3. De-noising Techniques

3.1 Adjustment of Measurement Configuration (AMC)

In a finite difference, the differential intervals, related to the density of measurement points in practical measurement, can largely affect the accuracy of difference. Assuming the distance between two adjacent measurement points is D_m, and the wavelength of vibration of beam under the current excitation is λ, the differential truncation error increases as a

result of increase in the value of D_m / λ, meaning the reduction of accuracy of difference; however, it is envisaged that the increase in D_m / λ will lead to reduction in noise level. This can be demonstrated in Fig. 3 for the discussed beam, in which the distributions of various DI^{exact} and DI^{noisy} against D_m / λ were displayed. It can thus be seen that, in order to reach a balance between the accuracy of difference and noise immunity, an appropriate value of D_m / λ should be selected, Fig. 3(c) among four candidate selections. In this case, location of the damaged zone is revealed clearly without any further de-noising treatment.

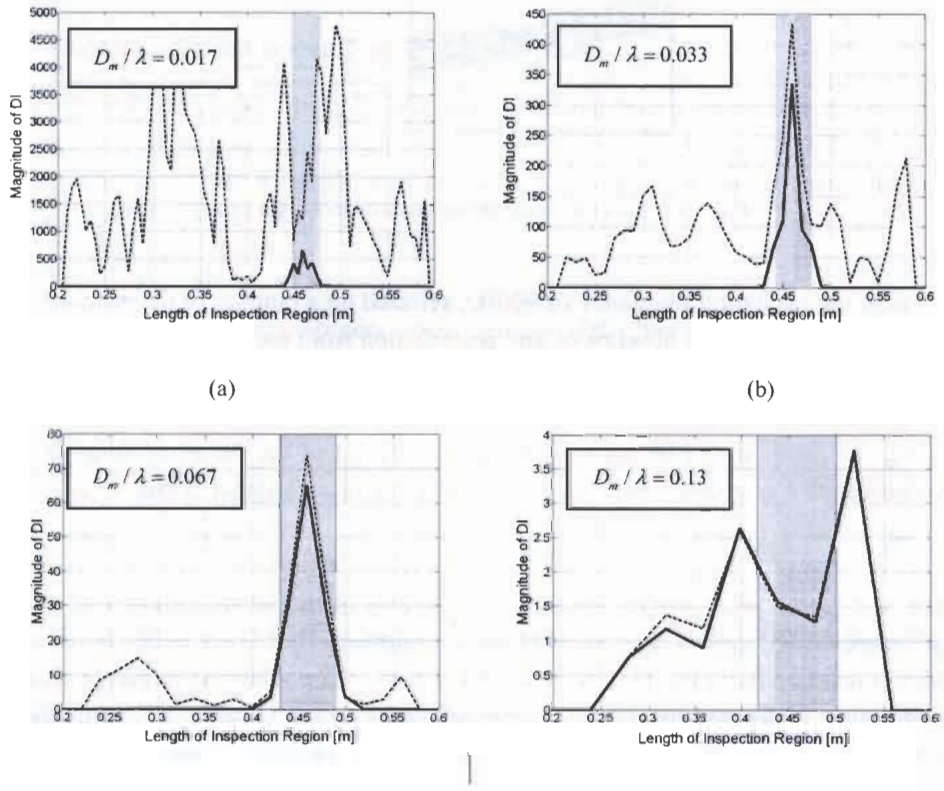

Fig. 3 Distributions of DI along with the increase of D_m / λ (solid line: DI^{exact}; dashed line: DI^{noisy}): (a) 0.017; (b) 0.033; (c) 0.067 and (d) 0.13

To further quantitatively describe the influence of D_m / λ on detection accuracy, two signal parameters, Accuracy of Difference (AD) and Noise Influence (NI), were introduced:

a. AD

An effective damaged zone is first defined, centralized at the center of the damaged zone and containing the peak values of DI^{exact} as a result of Dirac changes near damage boundaries, as shown in Fig. 3. Obviously the length of such an effective damaged zone is associated with D_m, and is in principle larger than the actual length of the damaged zone. Letting the maximum peak value of DI^{exact} within the effective damaged zone be *c*, the maximum peak value of DI^{exact} outside the effective zone be *t*, and the mean of all DI^{exact} throughout the inspection region be *a*, *AD* is then defined as

$$AD = \frac{t}{a} \tag{4a}$$

It can be better understood by re-arranging *AD* as

$$AD = \frac{t}{a} = \frac{t/c}{a/c} \tag{4b}$$

in which the numerator represents the relative fluctuation of DI^{exact} in the intact zone with regard to the maximum changes in the signal due to the presence of damage (c), and it additionally shows the relative dominance of the damage-induced changes in DI^{exact}. In particular, the smaller t/c is, the more prominent is DI^{exact} in the effective damaged zone. The denominator reflects the mean of all damage indices with regard to the maximum changes in the signal due to the presence of damage. Accuracy of the finite difference is deemed acceptable when $0 < AD \le 1$ (for example, those signals in Figs. 3(a)~(c), in which both the location and size of the damaged zone can be captured roughly; while the approach presents low accuracy when $AD > 1$ (for example, the signal in Fig. 3(d)), failing to describe the information related to damage.

b. *NI*

Along the same line of consideration for developing *AD*, the index, *NI*, is defined as,

$$NI = \frac{1-\Xi}{1-\Xi_c} \tag{5a}$$

where Ξ is the correlation coefficient between DI^{exact} and DI^{noisy}, which is

$$\Xi = \frac{N\sum_{i=1}^{N} \mathrm{DI}_i^{\mathrm{noisy}} \cdot \mathrm{DI}_i^{\mathrm{exact}} - \sum_{i=1}^{N} \mathrm{DI}_i^{\mathrm{noisy}} \cdot \sum_{i=1}^{N} \mathrm{DI}_i^{\mathrm{exact}}}{\sqrt{N\sum_{i=1}^{N} (\mathrm{DI}_i^{\mathrm{noisy}})^2 - (\sum_{i=1}^{N} \mathrm{DI}_i^{\mathrm{noisy}})^2} \cdot \sqrt{N\sum_{i=1}^{N} (\mathrm{DI}_i^{\mathrm{exact}})^2 - (\sum_{i=1}^{N} \mathrm{DI}_i^{\mathrm{exact}})^2}} \tag{5b}$$

where N is the number of measurement points in the inspection region. The greater the similarity between them, the closer to unity is the coefficient Ξ. In Eq. (5a), Ξ_c is a threshold, over which the measurement noise influence is deemed significant leading to poor recognizability of signals. When $0 < NI \le 1$ (i.e., $\Xi \ge \Xi_c$), DI^{exact} and DI^{noisy} exhibit high coincidence (for example, those signals in Figs. 3(c) and (d)), indicating that measurement noise become negligible; while when $NI > 1$ (i.e., $\Xi < \Xi_c$), DI^{noisy} deviates significantly from DI^{exact} (for example, those signals in Figs. 3(a) and (b)), making the identification impossible without applying any de-noising treatment.

From the above twofold discussion, it becomes clear that an ideal scenario is the case in which both *AD* and *NI* are as low as possible, or at least below the unity. In order to determine an optimal D_m / λ so as to ensure both *AD* and *NI* are in acceptable levels, signals shown in Fig. 3 were further processed to extract their corresponding *AD* and *NI* values. Figure 4(a) displays the variations in *AD* and *NI* under different selections of D_m / λ. The ascending trend for *AD* and descending trend for *NI* with the increase in D_m / λ reconfirm the previous observation and analysis. Most importantly, when D_m / λ is around 0.1, both *AD* and *NI* fall into acceptable levels ($0 < AD \le 1$ and $0 < NI \le 1$). Such a selection of $D_m / \lambda = 0.1$ corresponds to the case shown in Fig. 3(c) where roughly TEN measurement points per wavelength are used for constructing *DI*, reaching a compromise between signal recognizability and tolerance to measurement noise. In Fig. 3(c), damage can be estimated roughly even without application of any further signal de-nosing treatment. It is noteworthy that an optimal selection of D_m / λ is obviously dependent on the noise level. Fig. 4(b) and (c) present the variation of *AD-NI* curves under different initial noise levels that added to vibration displacements. In Eq. (3), by changing the deviations of Δw (keeping the variance of $\Delta\varphi$ to be 1°) and $\Delta\varphi$ (keeping the variance of Δw to be 1% of the magnitude of w^{exact}), respectively. It can be observed that when the measurement noise level is higher, *NI* becomes more dominant in determining the selection of D_m / λ. Under such a circumstance less measurement points should be used to enhance the noise immunity.

3.2 Low-pass wavenumber filtering

Another way of noise reduction included in the approach can be understood as a standard post-signal processing approach based on a spectrum analysis. The distribution of DI^{exact} and DI^{noisy} in the wavenumber domain, after a Fast Fourier Transform (FFT), is presented in Fig. 5(a), showing certain overlapping in between at lower wavenumbers and dominance of noise at higher wavenumbers. A low-pass filter is therefore designed as,

$$\begin{aligned} \tilde{h}(k) &= 1, \qquad (k \in [-k_c, +k_c]) \\ \tilde{h}(k) &= 0, \qquad (k \in [-\infty, -k_c] \cup [+k_c, +\infty]) \end{aligned} \tag{6}$$

where k is wavenumber; $\tilde{h}(k)$ the transfer function of an ideal filter in the wavenumber domain; k_c the cutoff wavenumber with a unit of $rad \cdot m^{-1}$, as indicated in Fig. 5(a). In addition, in order to minimize the influence from boundaries of the inspection region (known as the *Gibbs phenomenon*), a rectangular window is multiplicatively applied to the calculated DI_i prior to the above wavenumber filtering.

The filtered data was then reconstructed to spatial domain, and it is observed from Fig. 5(b) that the noise interference has been effectively reduced and the location of damage can be identified through the image of reconstructed DI^{noisy} (shown in dashed line in the figure).

3.3 Data fusion

Given the strong adaptability of the proposed detection technique and the diversity of de-noising treatments, plenty of data containing effective damage-associated features can be obtained by a very limit number of tests, to form a data pool for the further process by data fusion, providing more accurate detection results.

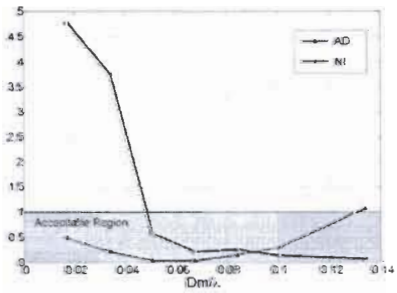

(a)

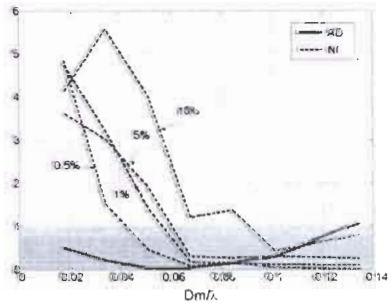

(b)

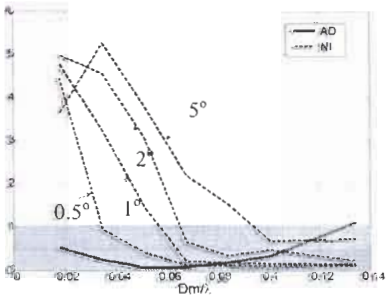

(c)

Fig. 4 *AD-NI* curves under (a) fixed noise level ($\Xi_c = 0.8$); and different noise levels by changing the (b) magnitudes (0.5%, 1%, 5% and 10%) and (c) phases (0.5°, 1°, 2°,and 5°) of initial noise level according to Eq. (3)

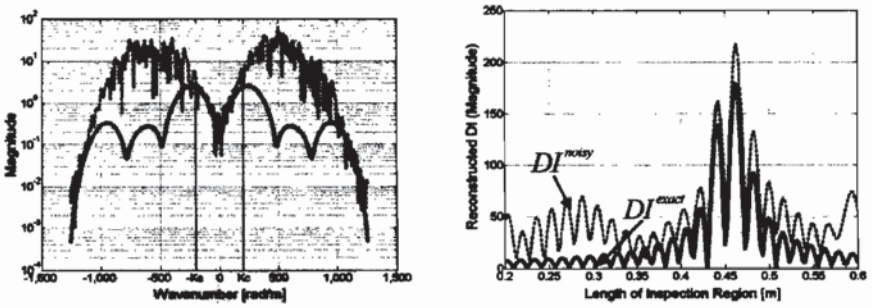

(a) (b)

Fig. 5 (a) Calculated DI^{exact} (dashed line) and DI^{noisy} (solid line) in wavenumber domain; (b) reconstructed DI^{exact} and DI^{noisy} upon application of a wavenumber filter ($k_c = 200 rad/m$)

Damage indices at measurement point i are obtained under K different measurement configurations, denoted by $\mathrm{DI}_{i-1}, \mathrm{DI}_{i-2}, \cdots, \mathrm{DI}_{i-L}, \cdots, \mathrm{DI}_{i-K}$ ($L = 1, 2, \cdots, K$), respectively, and all of them are subsequently amalgamated via a hybrid fusion scheme developed in authors' previous work [4, 5], defined as

$$\mathrm{DI}_{i\text{-hybrid}} = \mathrm{DI}_{i\text{-geometric}} \cap \mathrm{DI}_{i\text{-arithematic}} \tag{7}$$

where

$$\mathrm{DI}_{i\text{-geometric}} = \sqrt[K]{\mathrm{DI}_{i-1} \cdot \mathrm{DI}_{i-2} \cdots \mathrm{DI}_{i-L} \cdots \mathrm{DI}_{i-K}} \quad \text{and} \quad \mathrm{DI}_{i\text{-arithematic}} = \frac{1}{K}\sum_{L=1}^{K} \mathrm{DI}_{i-L} \tag{8}$$

$\mathrm{DI}_{i\text{-hybrid}}$ is the ultimate damage index at measurement point i upon data fusion.

4. Experimental validation

A simple cantilever beam was used in the experimental validation for easy understanding. The beam can be a component of a complex system consisting of various structural components. The Yong's Modulus of the beam is $70Gpa$ and the density is $2700kg/m^3$. The beam was 360mm long, 19mm wide and 6mm thick, introduced with a through-width notch by milling the beam to a 2mm reduction in its thickness serving as the damage. As shown in Fig. 6(a), the damaged zone was 8mm along the beam axis and the damage centre was 260mm away from the fixed end of the beam. An electro-mechanical shaker (B&K® 4809) was used to generate a harmonic excitation, applied 82mm away from the fixed end of the beam, as seen in Fig. 6(a). Within the inspection region with length of 240mm, out-of-plane displacements were captured at each measurement point using a scanning Doppler laser vibrometer system (Polytec® Scanning Vibrometer, PSV-400). There are four combinations of measurement configurations, corresponding to different frequencies of excitation and densities of measurement points along the inspection region, as shown in Table.1.

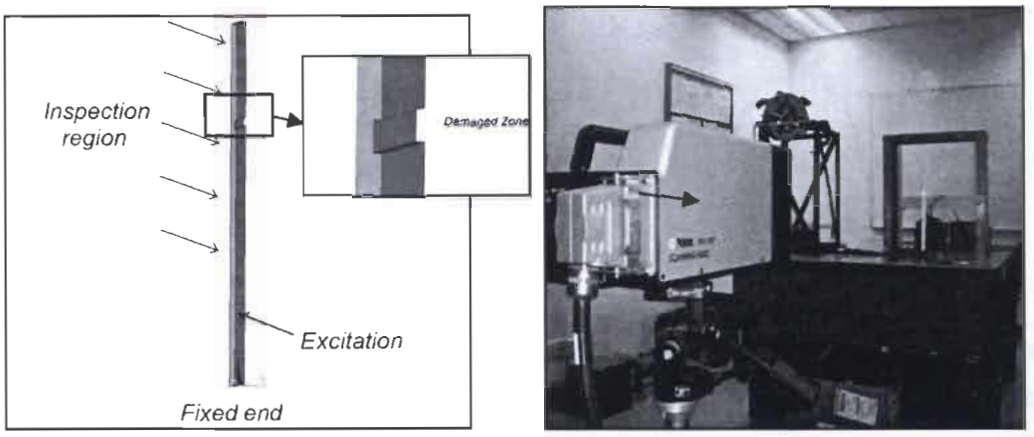

(a) (b)

Fig. 6 (a) schematic of the damaged beam under external harmonic excitation; and (b) experimental configuration

The detection results obtained under four different measurement configurations, as represented by case 1 to 4 in Tab.1, are presented from Fig. 7(a) to (d). It can be seen that the damaged zone cannot be clearly identified merely based on the measured raw data, corresponding to case 1, without any de-noising processing. Treated with the low-pass wavenumber filtering elaborated in Section 3.2 with cut-off wavenumber $k_c = 200$ rad/m, corresponding to case 2, the processed *DI* curve is shown in Fig. 7(b), from which the presence and location of the damaged zone can be recognized largely, demonstrating the effectiveness of the low-pass wavenumber filtering in handling practical noise-polluted signals. Then, using the measurement configuration according to case 3, i.e., by reducing the density of measurement points from 49 to 25 (but without applying wavenumber filtering), Fig. 7(c) exhibits the accordingly obtained *DI* curve, in which *DI* in the damaged zone clearly stood out compared with those in Fig. 7(b). This further supports previous conclusion drawn in Section 3.1 that, upon a proper choice of measurement parameters, the wavenumber filtering may not even be of necessity. Finally, Fig. 7(d) presents the *DI* curve after increasing the frequency of excitation from 140Hz to 903Hz (case 4), while keeping 25 measurement points and without applying wavenumber filtering, to also observe improvement in the detection accuracy, emphasizing the flexibility of the approach in implementation.

Table 1 · Four cases of measurement configurations

Case	Excitation frequencies (*Hz*)	Number of measurement points	Low-pass Wavenumber Filtering
1	140	49	Not used
2	140	49	Used
3	140	25	Not used
4	903	25	Not used

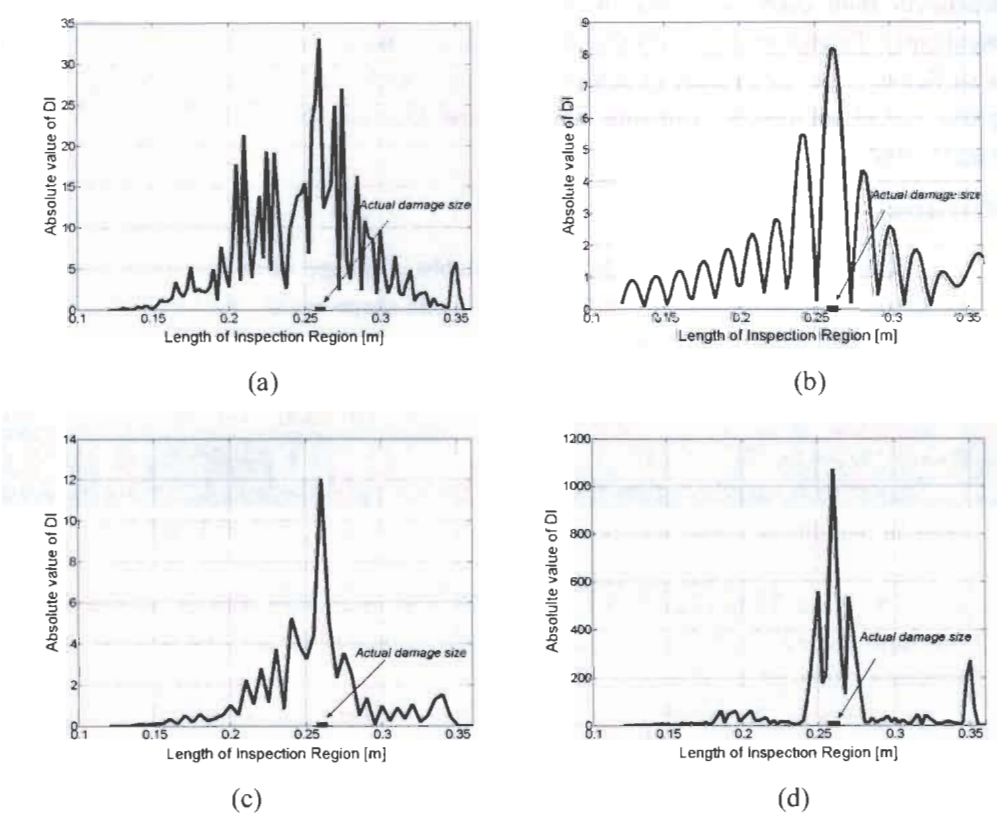

Fig. 7 DI distributions across the inspection region under different measurement configurations in Tab. 1

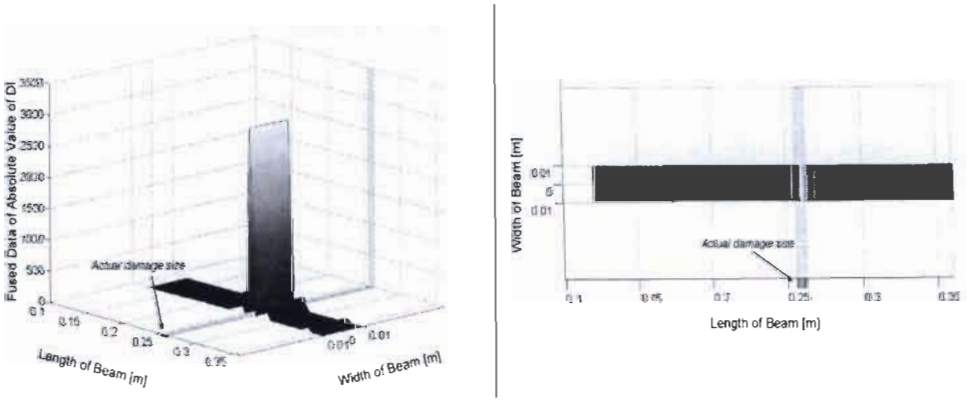

Fig. 8 (a) Three- and (b) two-dimensional presentation of the magnitude of fused DI

Finally, the above three *DI* plots (Figs. 7(b), (c) and (d)) were fused using the hybrid data fusion scheme described by Eq. (7), to obtain the ultimate *DI* curve, shown in Fig. 8. It is clear that the fused plot presents a much more explicit and intuitive indication of the presence and length of the damaged zone.

5. Conclusion

Development of noise reduction techniques for vibration-based method involving high-order derivatives of vibration signals were studied in this paper. It was discovered that by adjusting the configuration of measurement points, a balance between accuracy of difference and immunity of measurement noise can be achieved, providing important reference when conducting practical applications. Meanwhile, a standard post signal processing method based on low-pass wavenumber filtering, can also be deemed as an effective way to reducing the noise influence. The two developed methods were

independent from each other and are not necessary to be conducted simultaneously or subsequently. Thanks to the flexibility of de-noising approaches, a limited number of tests was sufficient to provide plenty of detection signals, which can be fused together to further improve calculated results, showing not only the location, but also exact size of the damaged zone.

References

(1) J. T. Kim, Y. S. Ryu, H. M. Cho and N. Stubbs, Damage identification in beam-type structures: frequency-based method vs. mode-shape-based method, Engineering Structures, Volume 25, 2003, pp.57-67

(2) A. K. Pandey, M. Biswas and M. M. Sammam, Damage detection from changes in curevature mode shapes, Journal of Sound and Vibration, Volume 145(2), 1991, pp.321-332.

(3) H. Xu, L. Cheng and Z. Su, Identification of structural damage based on locally perturbed dynamic equilibrium with an application to beam, Journal of Sound and Vibration (in press)

(4) Z. Su, X. Wang, L. Cheng, L. Yu and Z. Chen, On selection of data fusion schemes for structural damage evaluation, Structural Health Monitoring: An International Journal, Volume 8, 2009, pp.223-241.

(5) Z. Su, L. Cheng, X. Wang, L. Yu and C. Zhou, Predicting delamination of composite laminates using imaging approach, Smart Materials and Structures, Volume 18(7), 2009,074002(8pp).

Acknowledgements

L. Cheng and Z. Su wish to acknowledge the support given to them by the Hong Kong Polytechnic University (Research Grants G-U859 and A-PL08).